

3D-Consistent Image Inpainting with Diffusion Models

Leonid Antsfeld, Boris Chidlovskii

NAVER LABS Europe

<https://github.com/naver/croco-diffusion>

Abstract

We address the problem of 3D inconsistency of image inpainting based on diffusion models. We propose a generative model using image pairs that belong to the same scene. To achieve the 3D-consistent and semantically coherent inpainting, we modify the generative diffusion model by incorporating an alternative point of view of the scene into the denoising process. This creates an inductive bias that allows to recover 3D priors while training to denoise in 2D, without explicit 3D supervision. Training unconditional diffusion models with additional images as in-context guidance allows to harmonize the masked and non-masked regions while repainting and ensures the 3D consistency. We evaluate our method on one synthetic and three real-world datasets and show that it generates semantically coherent and 3D-consistent inpaintings and outperforms the state-of-art methods.

1. Introduction

Image inpainting refers to the task of filling in missing regions within an image [2,21] specified by a binary mask [10]. Such inpainted regions need to be semantically consistent and harmonized with the rest of the image. Moreover, inpainting methods need to handle various forms of masks where, in extreme cases, a vast majority of the image is missing. Any approach trained with a certain mask distribution can lead to poor generalization to novel mask types [15].

Recent advances in diffusion models led to image inpainting using Denoising Diffusion Probabilistic Models (DDPMs) [9,26]. The DDPM is trained to denoise the image by reversing a diffusion process. Starting from randomly sampled noise, it is iteratively applied for a certain number of steps and produces the final image sample; DDPMs have shown a strong capacity to generate diverse and high-quality 2D images [6,9,18]. Moreover, the problem of generalization to novel masks can be circumvented by inpainting that leverages *unconditionally trained* DDPMs [5,17]. Instead of learning a mask-conditional generative model, they condition the generation process by sampling from masked pixels during the reverse diffusion iterations. The unconditional DDPM is used as a generative prior to harmonize information between masked and non-masked regions, by performing forward diffusion of non-masked regions and reverse diffusion of masked ones, operating in pixel [17] or latent spaces [5]. This allows the network to generalize to any mask during inference.

Despite their impressive performance in generating photo-realistic 2D images, diffusion models still lack the 3D understanding during the generation process

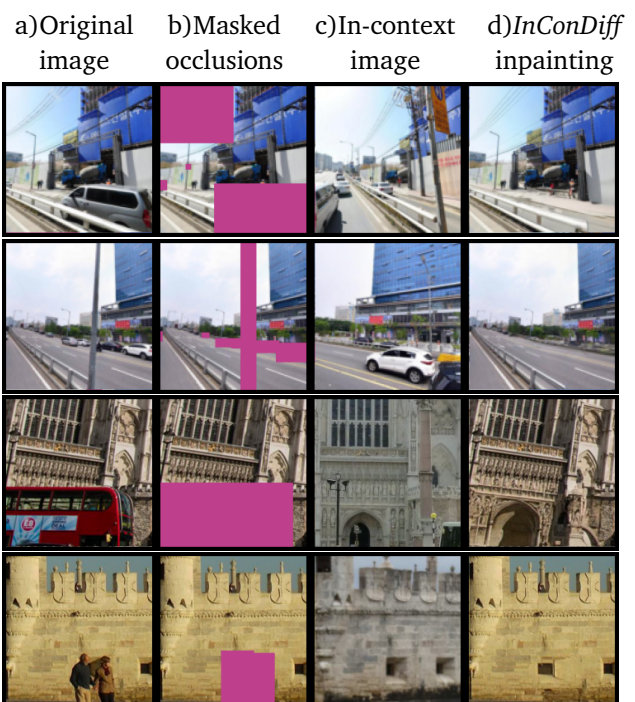


Figure 1: 3D-consistent inpainting with *InConDiff*: a) original image, b) image with masked occlusions; c) in-context image; d) *InConDiff* inpainting preserving 3D consistency.

[1,10,36]. Their inability to control the 3D properties of objects in the generated images is particularly harmful for image inpainting, which aims to harmonizing 3D properties of masked and non-masked regions. 3D understanding of diffusion models has been recently addressed by adding explicit 3D priors [10,13] or incorporating additional points of view [1]; however these methods require 3D supervision which is hard to ob-

tain [37].

In this paper, we address the problem of *3D-consistency of image inpainting* and propose *in-context inpainting* by injecting additional information into the image generative model, *without* 3D supervision. We train a generative model with image pairs that show the same scene and provide complementary information on the scene geometry, possibly under different lighting conditions. We exploit this complementarity when a part of the scene is occluded in one image but observed in another. At inpainting step, the model receives an image with a mask and inpaints the masked part while preserving the 3D scene information.

To achieve the 3D-consistent inpainting, we modify the generative diffusion model. We train our model by incorporating the additional point of view of the scene into the denoising process. This creates an inductive bias that allows to recover 3D priors while training to denoise in 2D, without explicit 3D supervision. Training unconditional diffusion models with additional images as in-context guidance allows us to harmonize the masked regions while inpainting and ensuring the 3D consistency. We evaluate our method, named *InConDiff*, on one synthetic (HM3D) and three real-world (MegaDepth, StreetView and WalkingTour) datasets and show that it generates semantically harmonized and 3D-consistent inpaintings outperforming the state-of-the-art methods. Figure 1 shows examples of inpainting with *InConDiff*, with occlusions caused by the presence of cars, buses and pedestrians.

Our contributions can be summarized as follows:

- We train an unconditional diffusion model with an additional image as the in-context guidance for image generation.
- We apply post-conditional generative approach to image inpainting where the mask on first image is given at the inference time; we modify the re-sampling schedule for harmonizing boundaries between masked and non-masked regions of the image.
- We prove its efficiency of *InConDiff* for image inpainting with semantic and random masks on one synthetic and three real-world datasets.

2. Related Work

Image Inpainting. The task of image inpainting inputs an image and a binary mask that defines the erased pixels [16, 33]. The original image pixels are removed and new ones are generated based on the mask. The domain of image inpainting was previously dominated by Generative Adversarial Networks (GANs) [11, 15,

21] that use an encoder-decoder architecture as the main inpainting generator, adversarial training, and tailored losses that aim at photo-realism [16, 32]. Most GAN-based models output deterministic results as these models are trained with reconstruction losses and improved stability [33, 35]. Recent GAN-based methods achieve diversity [12, 39]; however, trained on single object datasets, they are not extended to inpaint other scenes.

Image Conditional Diffusion Models. Recent advances in diffusion models and the high expressiveness of pretrained Denoising Diffusion Probabilistic Models [9, 18] led to using them as a prior for generic image inpainting. Sohl-Dickstein *et al.* [26] applied early diffusion models to inpainting. Song *et al.* [27] proposed a score-based formulation using stochastic differential equations for unconditional image generation, with an additional application to inpainting. Score-based diffusion models was applied to conditional image generation in [3] and extended it to multi-speed diffusion. Ho *et al.* [8] jointly train a conditional and an unconditional diffusion models and combine the resulting conditional and unconditional score estimates. Image-to-image translation with diffusion models was proposed in [24], with an application to inpainting.

Unconditional Diffusion Models. RePaint [17] was first to show that a pretrained unconditional diffusion model can inpaint images without mask-conditioned training. It modifies the denoising process to condition generation on the non-masked image content. Similarly, X-Decoder [40] processes an input image and textual together for referring segmentation. It proceeds to prompt-based segmentation and, when combined with diffusion models, can erase the segmented objects. LatentPaint [5] extended the denoising process from pixel to latent space. Trained and evaluated mostly on human face datasets, these models perform well on 2D inpainting however they perform poorly on street view images or indoor images with important scene geometry. In this paper, we are first to address 3D consistent image inpainting and to make an additional step by integrating additional images in the training unconditional DDPMs.

3. Diffusion Models for Image Inpainting

We first present an unconditional DDPM and describe injecting in-context images in the reverse diffusion process. Then, we introduce 3D-consistent harmonization of masked and non-masked regions and modify the re-sampling schedule to accelerate the reverse process for the mask-based inpainting.

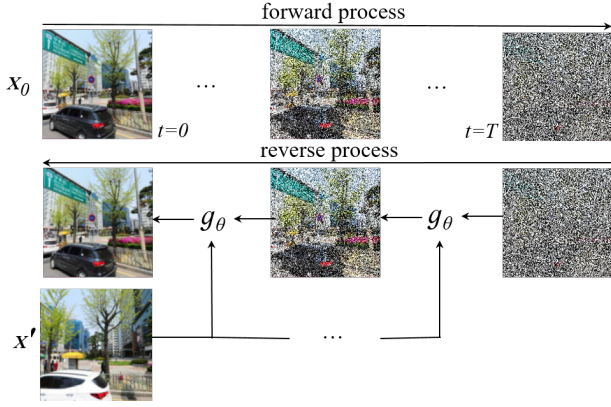


Figure 2: Unconditional DDPM with the forward process (right arrows) and the reverse denoising process (left arrows) that takes into account additional image \mathbf{x}' .

3.1. DDPMs

Diffusion models are designed to generate an image \mathbf{x}_0 by moving a starting full noise image $\mathbf{x}_T \sim \mathcal{N}(\mathbf{0}, \mathbf{I})$ progressively closer to the data distribution through multiple denoising steps $\mathbf{x}_{T-1}, \dots, \mathbf{x}_0$. The models are divided into forward and reverse diffusion processes. During the forward process, noisy images $\mathbf{x}_1, \dots, \mathbf{x}_T$ are created by repeatedly adding Gaussian noise starting from a training image \mathbf{x}_0 :

$$q(\mathbf{x}_t | \mathbf{x}_{t-1}) \sim \mathcal{N}(\mathbf{x}_t; \sqrt{1 - \beta_t} \mathbf{x}_{t-1}, \beta_t \mathbf{I}), \quad (1)$$

where β_t is a variance schedule that increases from $\beta_0 = 0$ to $\beta_T = 1$ and controls how much noise is added at each step. We initially use a cosine schedule [19] in our experiments and consider replacing it with alternative schedules in Section 3.3. The iterative process in (1) can be reshaped to directly obtain \mathbf{x}_t from \mathbf{x}_0 in a single step:

$$q(\mathbf{x}_t | \mathbf{x}_0) = \sqrt{\bar{\alpha}_t} \mathbf{x}_0 + \sqrt{1 - \bar{\alpha}_t} \epsilon$$

with $\epsilon \sim \mathcal{N}(\mathbf{0}, \mathbf{I})$, $\bar{\alpha}_t := \alpha_1 \dots \alpha_t$ and $\alpha_t := (1 - \beta_t)$. (2)

The reverse process aims at rolling back the steps of the forward process by finding the posterior distribution for the less noisy image \mathbf{x}_{t-1} given the more noisy image \mathbf{x}_t :

$$q(\mathbf{x}_{t-1} | \mathbf{x}_t, \mathbf{x}_0) \sim \mathcal{N}(\mathbf{x}_{t-1}; \boldsymbol{\mu}_t, \sigma_t^2 \mathbf{I}), \quad (3)$$

$$\text{where } \boldsymbol{\mu}_t := \frac{\sqrt{\bar{\alpha}_{t-1}} \beta_t}{1 - \bar{\alpha}_t} \mathbf{x}_0 + \frac{\sqrt{\bar{\alpha}_t} (1 - \bar{\alpha}_{t-1})}{1 - \bar{\alpha}_t} \mathbf{x}_t$$

$$\text{and } \sigma_t^2 := \frac{1 - \bar{\alpha}_{t-1}}{1 - \bar{\alpha}_t} \beta_t.$$

The image \mathbf{x}_0 being unknown, the distribution q can not be directly computed. Instead, DMs train a neural

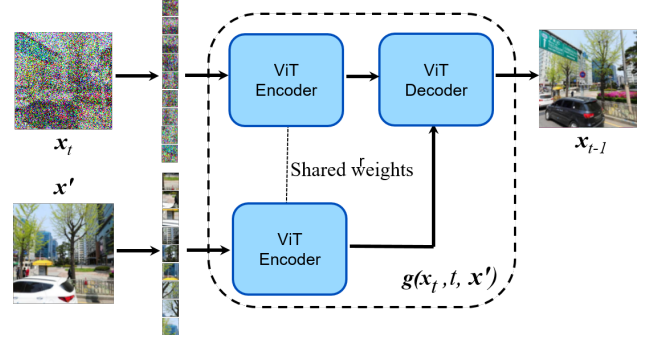


Figure 3: ViT architecture for learning the denoising model with additional image \mathbf{x}' .

network g with parameters θ to approximate q and predicts the parameters $\mu_\theta(\mathbf{x}_t, t)$ and $\Sigma_\theta(\mathbf{x}_t, t)$ of a Gaussian distribution:

$$p_\theta(\mathbf{x}_{t-1} | \mathbf{x}_t) = \mathcal{N}(\mathbf{x}_{t-1}; \mu_\theta(\mathbf{x}_t, t), \Sigma_\theta(\mathbf{x}_t, t)). \quad (4)$$

The learning objective for the model (4) is derived by considering the variational lower bound of the density assigned to the data by the model [9]. This approximate posterior is sampled at each generation step to progressively get the less noisy image \mathbf{x}_{t-1} from the more noisy image \mathbf{x}_t . It allows for a closed form expression of the objective since $q(\mathbf{x}_{t-1} | \mathbf{x}_t, \mathbf{x}_0)$ is also Gaussian.

Instead of predicting \mathbf{x}_0 , the seminal work of Ho *et al.* [9] proposed to predict the cumulative noise ϵ that is added to the current intermediate image \mathbf{x}_t . We use the following parametrization of the predicted mean $\mu_\theta(\mathbf{x}_t, t)$:

$$\mu_\theta(\mathbf{x}_t, t) = \frac{1}{\sqrt{\alpha_t}} \left(\mathbf{x}_t - \frac{\beta_t}{\sqrt{1 - \bar{\alpha}_t}} g_\theta(\mathbf{x}_t, t) \right) \quad (5)$$

and derive the following training objective

$$L_s = E_{t, \mathbf{x}_0, \epsilon} \|\epsilon - g_\theta(\mathbf{x}_t, t)\|^2. \quad (6)$$

Beyond the predicted mean, learning the variance $\Sigma_\theta(\mathbf{x}_t, t)$ in (4) of the reverse process reduces further the number of sampling steps and the inference time [18].

3.2. DDPMs with in-context images

We modify the training of unconditional DDPMs by injecting in-context images (see Figure 2) to better approximate the target distribution q and improve 3D consistency of image inpainting. Unlike the majority of generative diffusion models [9, 18] and inpainting methods [17, 34], which use U-Net backbones, we adopt the class of diffusion models based on Diffusion Transformers (DiTs) [22] which adhere to the best practices of Vision Transformers (ViTs) and make injecting of in-context image \mathbf{x}' straightforward.

By injecting the second image \mathbf{x}' , the objective function of our model is also to predict the cumulative noise ϵ that is added to the current intermediate image \mathbf{x}_t ,

$$L_2 = E_{t, \mathbf{x}_0, \epsilon} \|\epsilon - g_\theta(\mathbf{x}_t, t, \mathbf{x}')\|^2. \quad (7)$$

For training the network $g_\theta(\mathbf{x}_t, t, \mathbf{x}')$, we adopt the principle of *cross-view completion* which was shown to enable a network to perceive low-level geometric cues highly relevant to 3D vision tasks [28, 29]. The architecture of our network is shown in Figure 3. It takes an input the noised version of the first image \mathbf{x}_t and the clean version of image \mathbf{x}' . Both images are patchified and fed to an image encoder which is implemented using a ViT backbone. All patches from the second image are encoded using the same ViT encoder with shared weights. The latent token representations output by the encoder from both images are then fed to a decoder whose goal is to denoise \mathbf{x}_t . The decoder uses a series of transformer decoder blocks comprising cross-attention layers. This allows noised tokens from the first image to attend clean tokens from the second image, thus enabling cross-view comparison and reasoning. The model is trained using a pixel reconstruction loss over all patches, similar to CroCo [28, 29].

3.3. Conditioning DDPMs on the known region

At the inference step, we predict missing regions of an image defined by a mask region m ; we use the mask to condition the generative DDPM presented in the previous section. We first use DINOv2 [20] for detecting and masking the occlusion classes like e.g. *vehicle* and *pedestrian*; we then mask any patch containing at least 1 masked pixel. We follow [17] and denote the masked regions as $m \odot \mathbf{x}^m$ and the known (non-masked) regions as $(1 - m) \odot \mathbf{x}^k$. Since every reverse step (4) from \mathbf{x}_t to \mathbf{x}_{t-1} depends on \mathbf{x}_t , we can alter the known regions $(1 - m) \odot \mathbf{x}_t$ as long as we keep the correct properties of the target distribution. Since the forward process is defined by (1) as accumulative Gaussian noise, we can sample the intermediate image \mathbf{x}_t at any point in time using (4). This allows us to sample the known regions $m \odot \mathbf{x}_t$ at any time step t . Using (2) and (4) for the masked and known regions, respectively, one reverse step can be described by the following expression,

$$\begin{aligned} \mathbf{x}_{t-1}^k &\approx N(\sqrt{\alpha_t} \mathbf{x}_0, (1 - \alpha_t) \mathbf{I}) && \text{known regions} \\ \mathbf{x}_{t-1}^m &\approx N(\mu_\theta(x_t, t), \Sigma_\theta(x_t, t)) && \text{masked regions} \\ \mathbf{x}_{t-1} &= m \odot \mathbf{x}_{t-1}^m + (1 - m) \odot \mathbf{x}_{t-1}^k && \text{combined} \end{aligned} \quad (8)$$

Therefore, \mathbf{x}_{t-1}^k is sampled using the known regions in the image $m \odot \mathbf{x}_0$, while \mathbf{x}_{t-1}^m is sampled from the model, given the previous iteration \mathbf{x}_t . Then they are combined to the new sample \mathbf{x}_{t-1} .

Unfortunately, the basic denoising schedule (see Section 3.1) is insufficient for harmonizing the boundaries between masked and non-masked regions, due to restricted flexibility of sampling from both parts. RePaint [17] paid a particular attention to the noise schedule and shown that the model needs more time to harmonize the conditional information \mathbf{x}_{t-1}^k with the generated information \mathbf{x}_{t-1}^m before advancing to the next denoising step t . They introduced a *resampling* approach to harmonize the masked and non-masked input of the model. At an intermediate step, the resampling diffuses the output \mathbf{x}_{t-1} back to \mathbf{x}_t by sampling $\mathbf{x}_t \approx N(\sqrt{1 - \beta_t} \mathbf{x}_{t-1}, \beta_t \mathbf{I})$. By scaling back the output and adding noise, information incorporated in the generated region \mathbf{x}_{t-1}^m is still preserved in \mathbf{x}_t^m . It leads to a new \mathbf{x}_t^m which is both more harmonized with \mathbf{x}_t^k and contains conditional information from it. Figure 5 shows an example of inference process, with several phases of noise resampling jumps and diffusion.

Resampling with multiple jumps [17] archives the boundary harmonization between known and masked segments, however it requires extra time for inference. To reduce the inference time, we consider alternative noise schedules. We additionally modulate the number of jumps over the entire denoising process by measuring the smoothness of the intermediate representations as proposed in [4].

We modify the post-conditioned diffusion models by redefining the noise schedule, which is equivalent to importance sampling of the noise across different intensities. As demonstrated in [7], allocating more computation costs to intermediate noise levels yields superior performance compared to linearly increasing loss weights, particularly under constrained computational budgets. By running experiments and analyzing the performance of different noise schedules, including Laplace, Cauchy, Cosine and their shifted and scaled versions [7], we adopt the Laplace noise schedule which allows to reduce by half the overhead of multiple sampling from the distribution and the number of intermediate harmonization steps.

4. Experiments

We first present one synthetic and three real-world datasets used in the experiments. We also describe our approach to select image pairs suitable for training diffusion models with additional in-context images.

◦ *MegaDepth dataset* [14] consists of around 300K images downloaded from the web corresponding to 200 different landmarks. For each landmark, a point cloud model obtained using structure-from-motion (SfM) with COLMAP [25] is also provided.

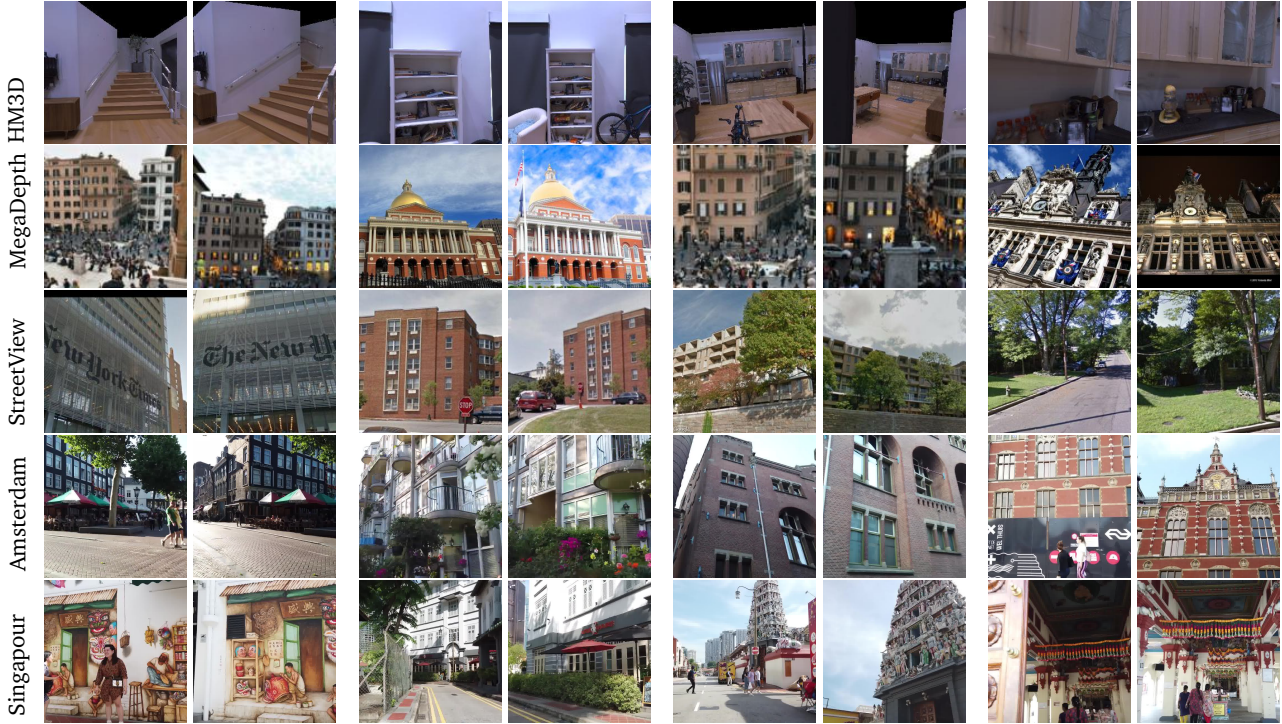


Figure 4: Image pairs for training unconditional DDPMs from HM3D, MegaDepth, StreetView and WalkingTour datasets.

- *Habitat-Matterport dataset (HM3D)* [23] is the large dataset of synthetically generated 3D indoor spaces. It consists of 1K high-resolution 3D scans (or digital twins) of building-scale residential, commercial, and civic spaces generated from real-world environments, all available with 3D meshes and camera poses.

- *StreetView dataset* contains 100K street view images from cities in South Korea, collected by Naver Maps¹. The images are provided with 3D location, camera pose and recording timestamps.

- *WalkingTour dataset*² is a collection of egocentric videos captured in urban environments from cities in Europe and Asia. It consists of 10 high-resolution videos, each showcasing a person walking through a urban environment.

All the datasets offer ways of getting information about the geometry of the scene and the camera poses. To be useful for training in-context diffusion models and inpainting, we use the geometry information for each dataset to extract image pairs that depict a scene with some partial overlap. In addition to reasonable overlap, we ensure good diversity of selected pairs. We follow [29] in obtaining an image pair quality score based on overlap and difference in viewpoint angle. Figure 4 shows examples of image pairs extracted from

all datasets.

Evaluation Metrics. We use three common evaluation metrics to assess the performance and effectiveness of inpainting methods[31].

The *Peak Signal to Noise Ratio (PSNR)* [30] is a widely used simple metric for evaluating the quality of image inpainting and reconstruction. It measures the ratio between the maximum possible power of a signal and the power of the noise present in the signal.

The *Learned Perceptual Image Patch Similarity (LPIPS)* [38] is a distance metric that is specifically designed to capture the perceptual similarity between two images. It is one of the most commonly used metrics for evaluating deep learning inpainting & restoration systems.

The *Structural Similarity Index (SSIM)* is a more advanced metric for evaluating the quality of image inpainting and reconstruction. It takes into account the human perception of image quality by measuring the structural similarity between two images, taking into account the luminance, contrast, and structure of the images.

Implementation details. Depth of the ViT encoder and decoder in *InConDiff* is 12 and 8, the number of heads is 12 and 16, respectively [29]. For every dataset, all images are resized to 256×256 ; the patch size is 8. The

¹<https://map.naver.com/>

²<https://shashankvkt.github.io/dora/>

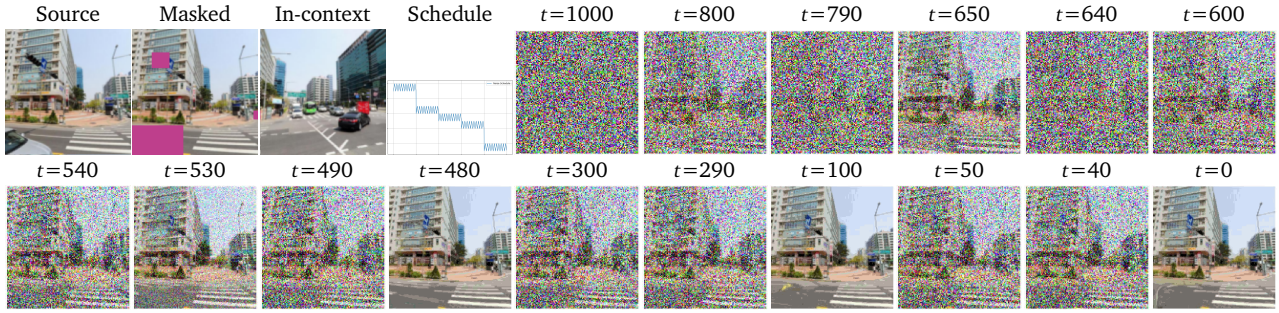


Figure 5: Inpainting with semantic mask using noise schedule with jumps. Note resampling effect for harmonization.

network is trained on image pairs from scratch, using AdamW optimizer, the fixed learning rate 0.0004, for 1000 epochs. During the inference, for both semantic and random masks, we apply the resampling with 1000 steps and 10 jumps.

4.1. Comparison to State-of-the-Art

We compare our *InConDiff* method to the state of the art RePaint method [17]. Due to unavailability of LatentPaint [5] at the submission deadline, we complete the comparison with two powerful inpainting models, the Stable Diffusion³ and Stable Diffusion XL⁴, known for excellent results on text- and mask-based inpainting of 2D images.

We note that RePaint [17] and LatentPaint [5] are trained and evaluated primarily on human face datasets, and they underperform on datasets with important presence of 3D geometry, both indoor (HM3D) and outdoor (MegaDepth, StreetView, WalkingTour).

We test our method with the *semantic mask* where obstacles are detected and masked as classes commonly representing obstacles such as *car*, *bus*, *bike*, *pedestrian*, *traffic light*, *pole*, etc. for outdoor scenes and *chair*, *armchair*, *table*, etc. for indoor scenes. Since considering certain class instances as obstacles (i.e. *table* for indoor, *pole* for outdoor scenes) is domain-specific and sometimes ambiguous, we also evaluate our method in a general case of *random mask*. Indeed, a randomly generated mask often covers multiple objects in different places of the scene, making the inpainting (both boundary harmonization and 3D consistency) harder. We proceed to the mask generation where a mask is a union of $n=10$ randomly selected rectangles, with the average masked ratio of 0.4 of the image size.

Tables 1-2 report quantitative results of comparison to the prior art on HM3D, MegaDepth, StreetView datasets

³<https://huggingface.co/runwayml/stable-diffusion-inpainting>

⁴<https://huggingface.co/diffusers/stable-diffusion-xl-1.0-inpainting-0.1>

Method	Semantic Mask			Random Mask		
	PSNR↑	LPIPS↓	SSIM↑	PSNR↑	LPIPS↓	SSIM↑
	MegaDepth					
RePaint [17]	20.73	0.24	0.87	18.22	0.31	0.79
SD	22.11	0.21	0.88	22.96	0.19	0.84
SD-XL	23.10	0.15	0.88	23.14	0.15	0.84
<i>InConDiff</i>	23.39	0.12	0.86	24.16	0.10	0.86
	StreetView					
RePaint [17]	17.92	0.30	0.81	17.16	0.34	0.78
SD	21.57	0.17	0.90	22.39	0.19	0.84
SD-XL	22.56	0.14	0.91	22.60	0.17	0.84
<i>InConDiff</i>	23.62	0.09	0.91	23.21	0.11	0.85
	HM3D					
RePaint [17]	19.62	0.24	0.88	18.67	0.35	0.82
SD	22.02	0.19	0.89	24.32	0.19	0.89
SD-XL	22.91	0.14	0.89	24.33	0.14	0.89
<i>InConDiff</i>	23.34	0.09	0.90	26.43	0.10	0.90

Table 1: Quantitative results on MegaDepth, StreetView and HM3D datasets, with both semantic and random masks.

and four scenes from WalkingTour dataset. RePaint [17] clearly underperforms on all datasets, due to mismatch between training and evaluation data. Our method outperforms SD and SD-XL models, trained for much longer and significantly larger datasets (see Supplementary), with both semantic and random masks. The gain is particularly important in complex real-world scenes, such as WalkingTour dataset.

Qualitative results. We complement the benchmark with visual inpainting examples for all datasets. In Figures 6- we present qualitative examples of inpainting for four datasets, with both semantic and random masks. Notice 3D consistency of inpaintings produced by our samples, and the overall harmonized boundaries between the masked and known regions.

Scene	Amsterdam			Istabil			Zurich			Stockholm		
Method	PSNR \uparrow	LPIPS \downarrow	SSIM \uparrow	PSNR \uparrow	LPIPS \downarrow	SSIM \uparrow	PSNR \uparrow	LPIPS \downarrow	SSIM \uparrow	PSNR \uparrow	LPIPS \downarrow	SSIM \uparrow
	Semantic Mask											
RePaint [17]	10.87	0.56	0.85	10.17	0.59	0.78	11.48	0.53	0.89	12.22	0.51	0.86
SD	14.09	0.54	0.84	14.64	0.23	0.77	15.14	0.21	0.90	17.41	0.16	0.85
SD-XL	14.03	0.24	0.84	13.69	0.24	0.78	15.17	0.22	0.90	17.49	0.16	0.86
<i>InConDiff</i>	19.96	0.09	0.89	17.30	0.13	0.83	21.75	0.06	0.93	19.70	0.09	0.89
	Random Mask											
RePaint [17]	10.68	0.60	0.70	10.39	0.60	0.70	11.19	0.58	0.71	12.37	0.55	0.72
SD	14.98	0.32	0.70	16.68	0.26	0.70	19.87	0.19	0.72	14.75	0.18	0.73
SD-XL	14.06	0.24	0.71	17.75	0.23	0.71	20.07	0.18	0.73	14.86	0.18	0.74
<i>InConDiff</i>	21.36	0.08	0.87	20.59	0.09	0.85	23.01	0.06	0.89	21.42	0.09	0.87

Table 2: Quantitative results on four scenes from WalkingTour dataset, with semantic and random masks.

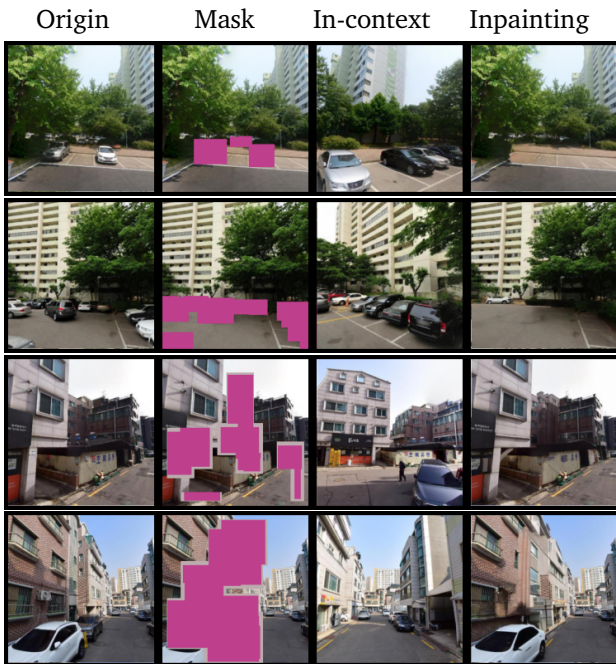


Figure 6: StreetView dataset: inpainting with semantic (top) and random (top) masks.

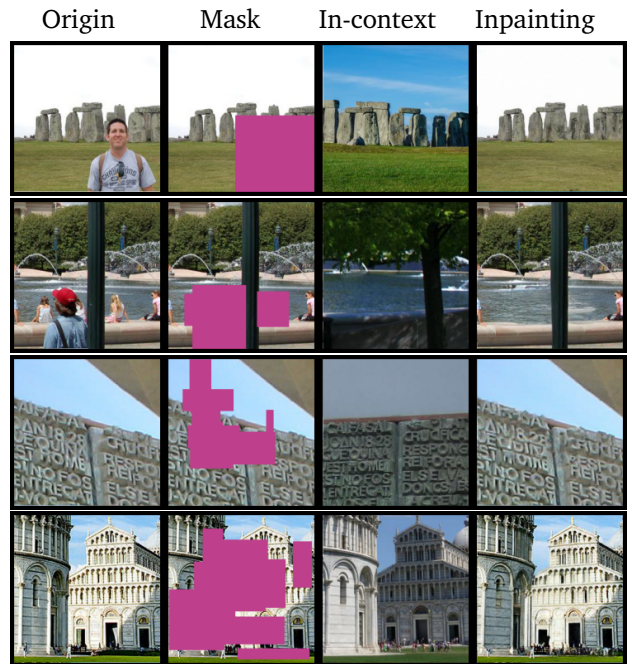


Figure 7: MegaDepth dataset: inpainting with semantic (top) and random (bottom) masks.

4.2. Ablation studies

Impact of masking ratio. In evaluation results with random masks in Tables 1-2, we generated the mask as a union of $n=10$ random rectangles, with the average mask ratio 0.4. Table 3 below ablates the average mask ratio by running *InConDiff* and SD-XL inpainting on MegaDepth dataset, with additional masking values 0.3, 0.5, 0.6 and 0.7. As the table shows, our *InConDiff* resists better than SD-XL to the larger random mask ratio, and benefits from the in-context images to fill in the masked segments.

Impact of sampling scheduler. Evaluation results presented in Tables 1-2 are reported for the resampling schedule with 1000 steps and 10 jumps, where the re-

Mask ratio	<i>InConDiff</i>			SD-XL		
	PSNR \uparrow	LPIPS \downarrow	SSIM \uparrow	PSNR \uparrow	LPIPS \downarrow	SSIM \uparrow
0.3	24.53	0.09	0.89	24.47	0.12	0.89
0.4	24.16	0.10	0.86	23.14	0.15	0.84
0.5	24.02	0.11	0.84	22.08	0.18	0.80
0.6	23.73	0.13	0.82	21.08	0.20	0.76
0.7	23.41	0.13	0.81	20.29	0.23	0.74

Table 3: Ablation on the average masking ratio for MegaDepth dataset.

sampling from the noisy version of better harmonization between the masked and unmasked regions. Table 4 shows ablation of both resampling parameters on the

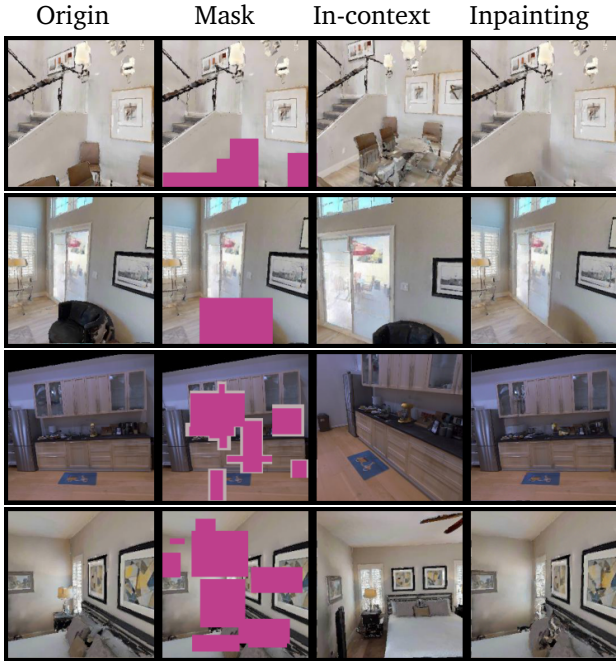


Figure 8: HM3D dataset: inpainting with semantic (top) and random (bottom) masks.

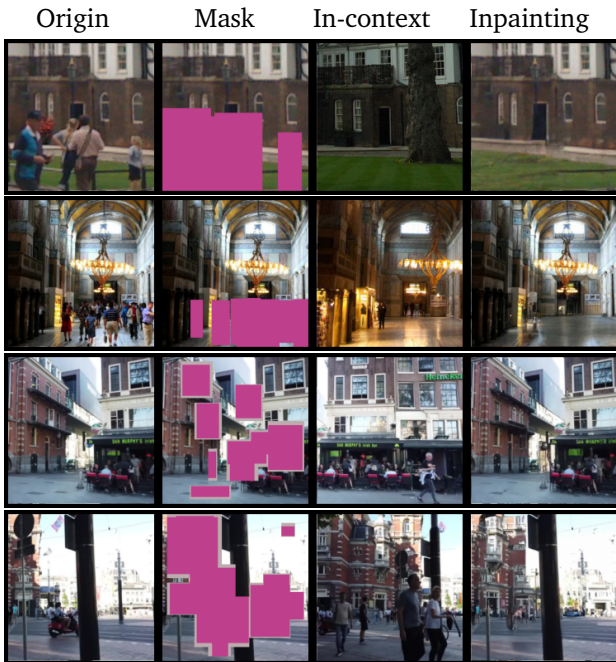


Figure 9: WalkingTour: inpainting with semantic (top) and random (bottom) masks.

HM3D dataset. It reports three main metrics for 250, 500, 1000 steps and 1, 5, 10 jumps. It shows that faster inpainting time comes with a small performance drop, with the number of jumps playing an important role.

Nsteps	250			500			1000		
Njumps	1	5	10	1	5	10	1	5	10
SSIM \uparrow	0.83	0.89	0.91	0.83	0.90	0.91	0.83	0.88	0.91
LPIPS \downarrow	0.26	0.12	0.10	0.26	0.11	0.09	0.26	0.11	0.09
PSNR \uparrow	18.7	23.2	24.1	18.7	23.7	25.1	18.7	23.7	25.1

Table 4: Ablation on resampling steps and jumps on HM3D dataset.

4.3. Limitations

Image inpainting with just an original image often leads to unrealistic off-context and hallucinations generated by diffusion models (some of such examples are shown and compared to *InConDiff* inpaintings in Supplementary). An additional viewpoint of the scene provides in-context guidance and injects 3D priors making inpainting more realistic and consistent. Unfortunately, it can be insufficient for reaching the goal in crowded real-world scenes. As result, inpainting can replace masked obstacles with other obstacles. This requires exploiting multi-view information when parts of the scene are observed in some frames but occluded in others. Extending one additional image by multiple ones will allow to address other challenges, like consistent object removal in videos, without 3D supervision.

5. Conclusion

We address the problem of 3D inconsistency of image inpainting based on diffusion models. We propose a generative model using image pairs that belong to the same scene. We modify the generative diffusion model by incorporating an alternative point of view of the scene into the denoising process. Training unconditional diffusion models with additional images as in-context guidance allows to harmonize masked and non-masked regions while repainting and ensures the 3D consistency. We evaluate our method on one synthetic and three real-world datasets and show that it generates semantically coherent and 3D-consistent inpaintings and outperforms the state-of-art methods. An additional viewpoint of the scene provides in-context guidance and injects 3D priors into the denoising process, reducing off-context hallucinations and making inpainting more realistic and 3D consistent, without 3D supervision.

References

- [1] Titas Anciukevicius, Zexiang Xu, Matthew Fisher, Paul Henderson, Hakan Bilen, Niloy J. Mitra, and Paul Guerrero. Renderdiffusion: Image diffusion for 3d reconstruction, inpainting and generation. In *IEEE Conference on Computer Vision and Pattern Recognition (CVPR)*, pages 12608–12618. IEEE, 2023. 1

- [2] Connelly Barnes, Eli Shechtman, Adam Finkelstein, and Dan B Goldman. Patchmatch: A randomized correspondence algorithm for structural image editing. *ACM Trans. Graph.*, 28(3):24, 2009. 1
- [3] Georgios Batzolis, Jan Stanczuk, Carola-Bibiane Schönlieb, and Christian Etmann. Conditional image generation with score-based diffusion models. *CoRR*, abs/2111.13606, 2021. 2
- [4] Ting Chen. On the importance of noise scheduling for diffusion models. *CoRR*, abs/2301.10972, 2023. 4
- [5] Ciprian Corneanu, Raghudeep Gadde, and Aleix M. Martinez. Latentpaint: Image inpainting in latent space with diffusion models. In *IEEE/CVF Winter Conference on Applications of Computer Vision (WACV)*, pages 4334–4343, 2024. 1, 2, 6
- [6] Prafulla Dhariwal and Alex Nichol. Diffusion models beat gans on image synthesis. *arXiv preprint arXiv:2105.05233*, 2021. 1
- [7] Tiankai Hang and Shuyang Gu. Improved noise schedule for diffusion training. *arXiv:2407.03297*, 2024. 4
- [8] Jonathan Ho and Tim Salimans. Classifier-free diffusion guidance, 2022. 2
- [9] Jonathan Ho, Ajay Jain, and Pieter Abbeel. Denoising diffusion probabilistic models. In *NeurIPS*, 2020. 1, 2, 3
- [10] Yi Huang, Jiancheng Huang, Yifan Liu, Mingfu Yan, Jiayi Lv, Jianzhuang Liu, Wei Xiong, He Zhang, Shifeng Chen, and Liangliang Cao. Diffusion model-based image editing: A survey. *arXiv:2402.17525*, 2024. 1
- [11] Jingyuan Li, Ning Wang, Lefei Zhang, Bo Du, and Dacheng Tao. Recurrent feature reasoning for image inpainting. In *Proceedings of the IEEE/CVF Conference on Computer Vision and Pattern Recognition*, pages 7760–7768, 2020. 2
- [12] Wenbo Li, Zhe Lin, Kun Zhou, Lu Qi, Yi Wang, and Jiaya Jia. Mat: Mask-aware transformer for large hole image inpainting. In *Proceedings of the IEEE/CVF conference on computer vision and pattern recognition*, pages 10758–10768, 2022. 2
- [13] Yuhan Li, Yishun Dou, Xuanhong Chen, Bingbing Ni, Yilin Sun, Yutian Liu, and Fuzhen Wang. Generalized deep 3d shape prior via part-discretized diffusion process. In *IEEE Conference on Computer Vision and Pattern Recognition (CVPR)*, pages 16784–16794, 2023. 1
- [14] Zhengqi Li and Noah Snavely. Megadepth: Learning single-view depth prediction from internet photos. In *IEEE Conference on Computer Vision and Pattern Recognition (CVPR)*, 2018. 4
- [15] Guilin Liu, Fitsum A Reda, Kevin J Shih, Ting-Chun Wang, Andrew Tao, and Bryan Catanzaro. Image inpainting for irregular holes using partial convolutions. In *Eur. Conf. Comput. Vis.*, pages 85–100, 2018. 1, 2
- [16] Guilin Liu, Aysegül Dundar, Kevin J Shih, Ting-Chun Wang, Fitsum A Reda, Karan Sapra, Zhiding Yu, Xi-aodong Yang, Andrew Tao, and Bryan Catanzaro. Partial convolution for padding, inpainting, and image synthesis. *IEEE Transactions on Pattern Analysis and Machine Intelligence*, 2022. 2
- [17] Andreas Lugmayr, Martin Danelljan, Andrés Romero, Fisher Yu, Radu Timofte, and Luc Van Gool. Repaint: Inpainting using denoising diffusion probabilistic models. In *IEEE Conference on Computer Vision and Pattern Recognition (CVPR)*, pages 11451–11461, 2022. 1, 2, 3, 4, 6, 7
- [18] Alex Nichol and Prafulla Dhariwal. Improved denoising diffusion probabilistic models. *arXiv preprint:2102.09672*, 2021. 1, 2, 3
- [19] Alex Nichol, Prafulla Dhariwal, Aditya Ramesh, Pranav Shyam, Pamela Mishkin, Bob McGrew, Ilya Sutskever, and Mark Chen. Glide: Towards photorealistic image generation and editing with text-guided diffusion models. *arXiv preprint:2112.10741*, 2021. 3
- [20] Maxime Oquab, Timothée Darcet, Théo Moutakanni, Huy Vo, Marc Szafranec, Vasil Khalidov, Pierre Fernandez, Daniel Haziza, Francisco Massa, Alaaeldin El-Nouby, Mahmoud Assran, Nicolas Ballas, Wojciech Galuba, Russell Howes, Po-Yao Huang, Shang-Wen Li, Ishan Misra, Michael Rabbat, Vasu Sharma, Gabriel Synnaeve, Hu Xu, Hervé Jegou, Julien Mairal, Patrick Labatut, Armand Joulin, and Piotr Bojanowski. Dinov2: Learning robust visual features without supervision. *arXiv:2304.07193*, 2024. 4
- [21] Deepak Pathak, Philipp Krahenbuhl, Jeff Donahue, Trevor Darrell, and Alexei A Efros. Context encoders: Feature learning by inpainting. In *IEEE Conf. Comput. Vis. Pattern Recog.*, pages 2536–2544, 2016. 1, 2
- [22] William Peebles and Saining Xie. Scalable diffusion models with transformers. In *IEEE/CVF International Conference on Computer Vision (ICCV)*, pages 4172–4182. IEEE, 2023. 3
- [23] Santhosh Kumar Ramakrishnan, Aaron Gokaslan, Erik Wijmans, Oleksandr Maksymets, Alexander Clegg, John M Turner, Eric Undersander, Wojciech Galuba, Andrew Westbury, Angel X Chang, Manolis Savva, Yili Zhao, and Dhruv Batra. Habitat-matterport 3d dataset (HM3d): 1000 large-scale 3d environments for embodied AI. In *Thirty-fifth Conference on Neural Information Processing Systems Datasets and Benchmarks Track*, 2021. 5
- [24] Chitwan Saharia, William Chan, Huiwen Chang, Chris A. Lee, Jonathan Ho, Tim Salimans, David J. Fleet, and Mohammad Norouzi. Palette: Image-to-image diffusion models. In *SIGGRAPH*, pages 15:1–15:10. ACM, 2022. 2
- [25] Johannes Lutz Schönberger and Jan-Michael Frahm. Structure-from-motion revisited. In *IEEE Conference on Computer Vision and Pattern Recognition (CVPR)*, 2016. 4
- [26] Jascha Sohl-Dickstein, Eric A. Weiss, Niru Maheswaranathan, and Surya Ganguli. Deep unsupervised learning using nonequilibrium thermodynamics. *arXiv:1503.03585*, 2015. 1, 2
- [27] Yang Song, Jascha Sohl-Dickstein, Diederik P. Kingma, Abhishek Kumar, Stefano Ermon, and Ben Poole. Score-based generative modeling through stochastic differential equations. *arXiv:2011.13456*, 2020. 2

-
- [28] P. Weinzaepfel, V. Leroy, T. Lucas, R. Brégier, Y. Cabon, V. Arora, L. Antsfeld, B. Chidlovskii, G. Csurka, and J. Revaud. CroCo: Self-Supervised Pretraining for 3D Vision Tasks by Cross-View Completion. In *NeurIPS*, 2022. 4
- [29] Philippe Weinzaepfel, Thomas Lucas, Vincent Leroy, Yohann Cabon, Vaibhav Arora, Romain Brégier, Gabriela Csurka, Leonid Antsfeld, Boris Chidlovskii, and Jérôme Revaud. Croco v2: Improved cross-view completion pre-training for stereo matching and optical flow. In *European Conference on Computer Vision (ECCV)*, 2023. 4, 5
- [30] Fei Xia, Amir R. Zamir, Zhiyang He, Alexander Sax, Jitendra Malik, and Silvio Savarese. Gibson env: Real-world perception for embodied agents. In *IEEE Conference on Computer Vision and Pattern Recognition (CVPR)*, pages 9068–9079, 2018. 5
- [31] Hanyu Xiang, Qin Zou, Muhammad Ali Nawaz, Xianfeng Huang, Fan Zhang, and Hongkai Yu. Deep learning for image inpainting: A survey. *Pattern Recognition*, 134: 109046, 2023. 5
- [32] Ahmet Burak Yildirim, Hamza Pehlivan, Bahri Batuhan Bilecen, and Aysegul Dundar. Diverse inpainting and editing with gan inversion. *arXiv preprint:2307.15033*, 2023. 2
- [33] Jiahui Yu, Zhe Lin, Jimei Yang, Xiaohui Shen, Xin Lu, and Thomas S Huang. Free-form image inpainting with gated convolution. In *Proceedings of the IEEE/CVF International Conference on Computer Vision*, pages 4471–4480, 2019. 2
- [34] Tao Yu, Runseng Feng, Ruoyu Feng, Jinming Liu, Xin Jin, Wenjun Zeng, and Zhibo Chen. Inpaint anything: Segment anything meets image inpainting. *arXiv preprint arXiv:2304.06790*, 2023. 3
- [35] Yongsheng Yu, Libo Zhang, Heng Fan, and Tiejian Luo. High-fidelity image inpainting with gan inversion. In *Computer Vision—ECCV 2022: 17th European Conference, Tel Aviv, Israel, October 23–27, 2022, Proceedings, Part XVI*, pages 242–258. Springer, 2022. 2
- [36] Guanqi Zhan, Chuanxia Zheng, Weidi Xie, and Andrew Zisserman. A general protocol to probe large vision models for 3d physical understanding. *arXiv:2310.06836*, 2024. 1
- [37] Guanhua Zhang, Jiabao Ji, Yang Zhang, Mo Yu, Tommi S. Jaakkola, and Shiyu Chang. Towards coherent image inpainting using denoising diffusion implicit models. In *ICML*, pages 41164–41193. PMLR, 2023. 2
- [38] Richard Zhang, Phillip Isola, Alexei A. Efros, Eli Shechtman, and Oliver Wang. The unreasonable effectiveness of deep features as a perceptual metric, 2018. 5
- [39] Shengyu Zhao, Jonathan Cui, Yilun Sheng, Yue Dong, Xiao Liang, Eric I Chang, and Yan Xu. Large scale image completion via co-modulated generative adversarial networks. *arXiv preprint:2103.10428*, 2021. 2
- [40] Xueyan Zou, Zi-Yi Dou, Jianwei Yang, Zhe Gan, Linjie Li, Chunyuan Li, Xiyang Dai, Harkirat Behl, Jianfeng Wang, Lu Yuan, et al. Generalized decoding for pixel, image, and language. *arXiv preprint:2212.11270*, 2022. 2
-